

International Journal of Modern Physics D  
 © World Scientific Publishing Company

## Consistency of nonlinear interacting ghost dark energy with recent observations

E. Ebrahimi

*Faculty of Physics, Shahid Bahonar University,  
 Kerman, PO Box 76175, Iran;*

*Research Institute for Astronomy and Astrophysics of Maragha (RIAAM), Maragha, Iran  
 ebrahimi@uk.ac.ir*

H. Golchin

*Faculty of Physics, Shahid Bahonar University,  
 Kerman, PO Box 76175, Iran*

*h.golchin@uk.ac.ir*

A. Mehrabi

*Department of Physics, Bu-Ali Sina University, Hamedan 65178, 016016, Iran  
 Mehrabi@basu.ac.ir*

S. M. S. Movahed

*Department of Physics, Shahid Beheshti University, G.C., Evin, Tehran 19839, Iran  
 School of Physics, Institute for Researches in Fundamental Sciences (IPM), P.O.Box  
 19395-5531, Tehran, Iran  
 m.s.movahed@ipm.ir*

Received Day Month Year

Revised Day Month Year

In this paper we investigate ghost dark energy model in the presence of non-linear interaction between dark energy and dark matter. We also extend the analysis to the so called generalized ghost dark energy (GGDE) which  $\rho_D = \alpha H + \beta H^2$ . The model contains three free parameters as  $\Omega_D, \zeta (= \frac{8\pi G\beta}{3})$  and  $b^2$  (the coupling coefficient of interactions). We propose three kinds of non-linear interaction terms and discuss the behavior of equation of state, deceleration and dark energy density parameters of the model. We also find the squared sound speed and search for signs of stability of the model. To compare the interacting GGDE model with observational data sets, we use more recent observational outcomes, namely SNIa from JLA catalog, Hubble parameter, baryonic acoustic oscillation and the most relevant CMB parameters including, the position of acoustic peaks, shift parameters and redshift to recombination. For GGDE with the first non-linear interaction, the joint analysis indicates that  $\Omega_D = 0.7192 \pm 0.0062$ ,  $b^2 = 0.146^{+0.030}_{-0.026}$  and  $\zeta = 0.104 \pm 0.047$  at 1 optimal variance error. For the second interaction, the best fit values at  $1\sigma$  confidence are  $\Omega_D = 0.72091 \pm 0.0065$ ,  $b^2 = 0.0395 \pm 0.0080$  and  $\zeta \leq 0.0173$ . According to combination of all observational data sets considered in this paper the best fit values for third non-linearly interacting model are  $\Omega_D = 0.7287 \pm 0.0062$ ,  $b^2 = 0.0109 \pm 0.0023$  and  $\zeta \leq 0.00764$  at  $1\sigma$  confidence interval. Finally we found that the presence of interaction is compatible in mentioned models via current observational

2 *E. Ebrahimi, H. Golchin, A. Mehrabi, S. M. S. Movahed*

datasets.

*Keywords:* Ghost dark energy; Non-linear interaction; Observational cosmology.

PACS numbers:

## 1. Introduction

Accelerating expansion of the universe is a mysterious event in the modern cosmology. The most relevant observational results based on SNIa as robust standard candle around 1998 demonstrated that our universe is experiencing an accelerative phase of expansion at the late time.<sup>1–4</sup> After that, other observational data sets provided by cosmic microwave background (CMB)<sup>5–8</sup> and large scale structure as well as baryon acoustic oscillation<sup>9–15</sup> favored mentioned acceleration phase. On the other hand, there are many models to achieve the late time acceleration epoch for evolution of our universe. In a more general and famous approach, the responsible for mentioned phase is generically relegated to the influence of a strange form of energy which is the so-called dark energy (DE). The simplest candidate for this approach is cosmological constant.<sup>16–19</sup> Such proposal is noticeable in the case that the right underlying theory of gravity is supposed to be general relativity (GR). Moreover there are some approaches to modify gravity in cosmological scales, in order to include the late time accelerating epoch.<sup>20–23</sup> Dynamical models of dark energy (models with time varying equation of state parameter) are also allowed from theoretical point of view, such models are supported by observational evidences. An incomplete list of examples includes time varying cosmological constant,<sup>24</sup> quintessence,<sup>25–29</sup> phantom fields,<sup>30–35</sup> holographic dark energy which originate from quantum gravity approach,<sup>36–41</sup> age graphic dark energy<sup>42–44</sup> and so on. An interesting problem which potentially can be resolved in dynamical approach is the so-called “coincidence problem”, which simply asks “why dark energy component becomes dominant at present time?”.

Ghost dark energy (GDE), is another dynamical DE model introduced in.<sup>45,46</sup> GDE is based on the Veneziano ghost field which has already been introduced to solve the  $U(1)$  problem in  $QCD$  theory.<sup>47–51</sup> In a Minkowskian spacetime there is not any observable consequence from the ghost field but turning into a dynamical spacetime the ghost field affects the vacuum energy density.

In the lowest level, ghost dark energy contribution to the vacuum energy density can be taken as  $\Lambda_{QCD}^3 H$ , where  $H$  is the Hubble parameter and  $\Lambda_{QCD}^3$  is QCD mass scale.<sup>46</sup> In,<sup>45,52</sup> authors showed that this contribution is enough to drive an acceleration in the cosmic background. Considering the values  $\Lambda_{QCD} \sim 100 MeV$  and  $H \sim 10^{-33} eV$  one obtains  $\Lambda_{QCD}^3 H \sim (3 \times 10^{-3} eV)$  which solve the fine tuning problem.<sup>46</sup> Another interesting feature of this model is that there is no need to introduce new degrees of freedom since GDE is totally embedded in the known physics. Different features of GDE is extensively studied.<sup>53–59</sup>

The influence of the ghost field to the vacuum energy density was reconsidered

in reference.<sup>60</sup> They found that, there exists a second order term proportional to  $H^2$  which can contribute to the vacuum energy density. Accordingly, the ghost dark energy density can be redefined as<sup>60</sup>  $\rho_D = \alpha H + \beta H^2$  where  $\alpha$  and  $\beta$  are constants. The dark energy model which is based on this relation is called generalized ghost dark energy (GGDE). According to previous results represented in<sup>60,61</sup> considering GGDE model, the second order term ( $\beta H^2$ ) has opposite dynamical influence with respect to the linear term ( $\alpha H$ ). Subsequently, one can expect that some problems with GDE will be removed in the generalization approach.

As mentioned before, cosmological constant or in brief  $\Lambda$  is one of the first candidates can explain dynamical evolution of the universe with accelerating expansion rate. In the standard model of cosmology entitled  $\Lambda$ CDM, dark sectors namely, DE ( $\Lambda$ ) and dark matter (DM) evolve separately and do not interact. However, because of the unclear nature of both DE and DM, it is possible to consider interaction between the dark sectors in the universe and there is not any theoretical reason against such an interaction.<sup>25</sup> Interacting models are also capable to solve the coincidence problem. There also exists observational evidences which support the interacting models.<sup>62,63</sup>

Considering a typical interaction between DE and DM, there will arise a simple question that what the form of the interaction term is? Phenomenologically one can choose the interaction terms as a linear combination of  $\rho_D$  and  $\rho_m$  at the simplest level. However one can ask why just linear choices? when we work on GDE and GGDE models with a linear regime they suffer a negative sound speed. Seeking a solution to this problem and also looking for better consistency with observations, one can consider non-linear interacting models. Non-linear interacting models of DE have been introduced and studied in the literature.<sup>64,65</sup> Also authors of<sup>66</sup>, showed that a product coupling, i.e., an interaction term which is proportional to the product of  $\rho_D$ ,  $\rho_m$  and  $\rho_D + \rho_m$  can be consistent with observations. Next in,<sup>67</sup> Arevalo et al. proposed a general form of non-linear interaction term and studied the cosmic dynamics of the universe in presence of such an interaction term. For special cases of the non-linear interaction term they found analytic solutions which is consistent with the supernova type Ia (SNIa) data from the Union2 set. We will try almost a same choices of non-linear interaction terms in the GDE frame work.

Our aim in this paper is to consider a new form of non-linear interaction term seeking better agreement with observations and improving model defects such as stability. Observational consistency check has vital role not only for either to accept or to rule out underlying model but also for doing reliable comparison between different proposed theoretical models for describing the universe. Therefore, in this paper we put observational constraints on the free parameters of our interacting dynamical dark energy model. The most recent data for SNIa Joint Light-curve Analysis (JLA) sample will be considered. Also to make more completeness, we use Hubble parameter for different redshift from OHD dataset. Various measurements for determining the Baryon Acoustic Oscillation (BAO) including Sloan Digital Sky

4 *E. Ebrahimi, H. Golchin, A. Mehrabi, S. M. S. Movahed*

Survey (SDSS), Baryon Oscillation Spectroscopic Survey (BOSS), WiggleZ survey and 6dFGS survey are included. The major contribution of DE is at late epoch so here we consider the position of sound horizon, shift parameter and redshift of recombination from CMB observation, nevertheless it is possible to use CMB power spectrum to do much more completed evaluation. Finally, the joint analysis of all mentioned observational data to determine the best fit values for model free parameters has been done. As an other interesting investigation, one can explore the influence of GDE on the large scale structure in the universe, which will be done in separate work. One can find some examples for comparison of dark energy models with different observational data sets in.<sup>68–76</sup>

This paper is outlined as follows. In the next section, we review linear interacting and non-interacting GGDE models in a flat universe. Section 3 is devoted to extension from linear to non-linear interaction. In section 4 we will rely on the most recent observational data to check the consistency of our model. To this end, following indicators will be taken into account: SNIa from JLA observations, Hubble parameter, Baryonic Acoustic oscillation and CMB observational quantities including shift parameter, location of the first peak and redshift to recombinations. We summarize our results in section 5.

## 2. GGDE model with a general interaction term in flat universe

In this section we review GGDE model in general case. We will focus on the absence and presence of an interaction term between dark sectors of our universe. In this paper we limit ourself to influence of GGDE on the background evolution of universe and for the sake of clarity, as a beginning task we start with the Friedmann equation in a flat universe:

$$H^2 = \frac{8\pi G}{3} (\rho_r + \rho_m + \rho_D), \quad (2.1)$$

where  $\rho_r$ ,  $\rho_m$  and  $\rho_D$  are the energy densities of radiation, pressure-less matter (including dark and baryonic) and dark energy, respectively. According to the GGDE model,<sup>60</sup> the energy density of the dark energy defined by:

$$\rho_D = \alpha H + \beta H^2. \quad (2.2)$$

The dimensionless energy density of various components are:

$$\begin{aligned} \Omega_m &\equiv \frac{\rho_m}{\rho_{cr}} = \frac{8\pi G \rho_m}{3H^2}, \\ \Omega_D &\equiv \frac{\rho_D}{\rho_{cr}} = \frac{8\pi G(\alpha + \beta H)}{3H}, \\ \Omega_r &\equiv \frac{\rho_r}{\rho_{cr}} = \frac{8\pi G \rho_r}{3H^2}. \end{aligned} \quad (2.3)$$

where  $\rho_{cr} = 3H^2/(8\pi G)$ , so the first Friedmann equation can be written as  $\Omega_r + \Omega_m + \Omega_D = 1$ . Here we assume that a coupling term ( $Q$ ) exists between dark energy

and dark matter components. So the energy conservation equations read as:

$$\dot{\rho}_m + 3H\rho_m = Q, \quad (2.4)$$

$$\dot{\rho}_D + 3H\rho_D(1 + w_D) = -Q, \quad (2.5)$$

$$\dot{\rho}_r + 3H\rho_r(1 + w_r) = 0,$$

where  $w_D = \frac{P_D}{\rho_D}$  and  $w_r = 1/3$ . Summing above equations one finds the total energy density conservation equation:  $\dot{\rho} + 3H(\rho + P) = 0$ , where  $\rho = \rho_r + \rho_m + \rho_D$  and the total pressure equals  $P = P_r + P_D$ . However we consider interaction between dark sectors of our cosmos, since pressure is determined by kinetic considerations, therefore it is possible to have particle production (annihilation) without changing to functional form of pressure. Also according to *a priori* information from observations we consider pressureless dark matter in our analysis. The effective equation of state for dark matter determined by continuity equation, Eq. (2.4), equates to  $w_m^{\text{eff}} \equiv -Q/3H\rho_m$  and for dark energy according to Eq. (2.5), we have  $w_D^{\text{eff}} \equiv w_D + Q/3H\rho_D$ .<sup>77,78</sup> Taking the time derivative of (2.1) we find:

$$\dot{H} = -4\pi G\rho_D[y(1 + w_r) + 1 + u + w_D], \quad (2.6)$$

where  $y = \rho_r/\rho_D$  and  $u = \rho_m/\rho_D$ . Differentiating (2.2) with respect to time and also replacing  $\dot{H}$  from (2.6), we reach the following relation

$$\dot{\rho}_D = -4\pi G\rho_D[y(1 + w_r) + 1 + u + w_D](\alpha + 2\beta H), \quad (2.7)$$

so the conservation equation for DE (2.5), takes to the form

$$4\pi G u(\alpha + 2\beta H) - \frac{Q}{\rho_D} = (1 + w_D)[3H - 4\pi G(\alpha + 2\beta H)] - 4\pi G y(1 + w_r)(\alpha + 2\beta H), \quad (2.8)$$

now introducing  $\zeta \equiv \frac{8\pi G\beta}{3}$  and using the following relation

$$\frac{4\pi G}{3H}(\alpha + 2\beta H) = \frac{\Omega_D + \zeta}{2}, \quad (2.9)$$

which is obtained from  $\Omega_D$  in (2.3), it is possible to rewrite (2.8) as

$$u(\Omega_D + \zeta) - \frac{2Q}{3H\rho_D} = (1 + w_D)(2 - \Omega_D - \zeta) - y(1 + w_r)(\Omega_D + \zeta), \quad (2.10)$$

finally, noticing that  $u = \frac{\Omega_m}{\Omega_D} = \frac{1}{\Omega_D} - 1$ , the equation of state parameter  $w_D$  can be obtained as

$$w_D = \frac{\zeta - \Omega_D - Q'\Omega_D - \Omega_r\Omega_D - \zeta\Omega_r + y(1 + w_r)(\Omega_D + \zeta)\Omega_D}{\Omega_D(2 - \Omega_D - \zeta)}, \quad (2.11)$$

$$Q' = \frac{2Q}{3H\rho_D}.$$

Now let us turn to the deceleration parameter which is defined in terms of scale factor  $a$ , as:

$$q = -\frac{a\ddot{a}}{\dot{a}^2} = -1 - \frac{\dot{H}}{H^2}, \quad (2.12)$$

6 *E. Ebrahimi, H. Golchin, A. Mehrabi, S. M. S. Movahed*

substituting  $\dot{H}$  from (2.6) and using the definition of  $\Omega_D$  in (2.3), one can find

$$q = -1 + \frac{3}{2} \Omega_D [y(1 + w_r) + 1 + u + w_D]. \quad (2.13)$$

Using the relation  $\dot{\Omega}_D = H \frac{d\Omega_D}{d \ln a}$  one obtains the evolution of DE density parameter as  $\frac{d\Omega_D}{d \ln a} = -\frac{8\pi G\alpha}{3H} \frac{\dot{H}}{H^2}$ , noting (2.9), the evolution of  $\Omega_D$  can be written as:

$$\frac{d\Omega_D}{d \ln a} = \frac{4\pi G\alpha}{H^2(\alpha + \beta H)} [y(1 + w_r) + 1 + u + w_D]. \quad (2.14)$$

Since we are interested in late time universe, the contribution of radiation is negligible. In this case, the above equation can be written as:

$$\frac{d\Omega_D}{d \ln a} = \frac{3}{2} (\Omega_D - \zeta)(1 + w_D \Omega_D). \quad (2.15)$$

Hereafter we consider  $\Omega_r \rightarrow 0$  in all relevant equations, however for observational consideration, where the radiation has important contribution we will keep radiation density in relevant equations. Till now, we have shown the results in terms of a general form  $Q$  for interaction between DE and DM. To test the validity of the above results, we find the cosmological parameters  $w_D$  and  $q$  for some definite interactions. In the case of non-interacting model, setting  $Q = Q' = 0$  in (2.11), (2.13); we find

$$w_D = \frac{\zeta - \Omega_D}{\Omega_D(2 - \Omega_D - \zeta)}, \quad q = \frac{1}{2} + \frac{3}{2} \frac{\zeta - \Omega_D}{2 - \zeta - \Omega_D}, \quad (2.16)$$

which are in agreement with the respective relations obtained in.<sup>61</sup> Another model for interaction is  $Q = 3b^2 H(\rho_m + \rho_D) = 3b^2 H \rho_D(1 + u)$ . This interaction is linear in terms of  $\rho$ , with a coupling constant  $b^2$ . In this case one finds that  $Q' = \frac{2b^2}{\Omega_D}$ . Substituting this value to (2.11) and (2.13) leads to:

$$w_D = \frac{\zeta - \Omega_D - 2b^2}{\Omega_D(2 - \Omega_D - \zeta)}, \quad (2.17)$$

$$q = \frac{1}{2} + \frac{3}{2} \frac{\zeta - \Omega_D - 2b^2}{2 - \zeta - \Omega_D}, \quad (2.18)$$

and the evolution equation for energy density of DE is given by:

$$\frac{d\Omega_D}{d \ln a} = 3\Omega_D \left[ \frac{1 - \Omega_D}{2 - \Omega_D - \zeta} \left( 1 + \frac{2b^2}{\Omega_D} - \frac{\zeta}{\Omega_D} \right) - \frac{b^2}{\Omega_D} \right], \quad (2.19)$$

which are the same as the results in<sup>61,79</sup>. In the next section we will consider some new non-linear functional forms for interaction between dark matter and dark energy.

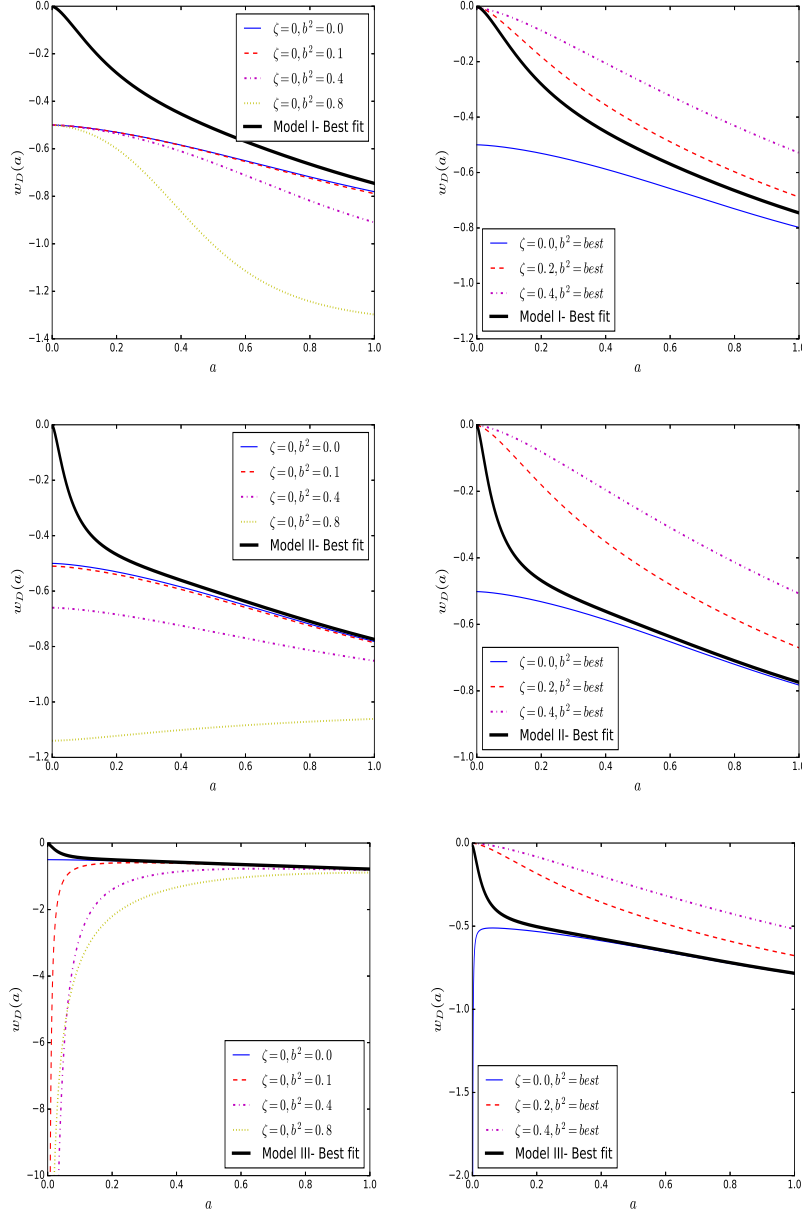


Fig. 1. The evolution of  $w_D$  as a function of scale factor for three models explained in the text. Left panels are devoted to  $\zeta = 0$ , while right panels correspond to best fit value for  $b^2$  based on joint analysis of SNIa+Hubble+BAO+CMB. Here we consider scale factor at present time as  $a_0 = 1$ . The value of  $\Omega_D$  at the present time is 0.70. In all plots the dark solid line corresponds to the best fit values determined by joint analysis. For the first model  $\Omega_D = 0.7192^{+0.0062}_{-0.0062}$ ,  $b^2 = 0.146^{+0.030}_{-0.026}$  and  $\zeta = 0.104^{+0.044}$ . For the second model  $\Omega_D = 0.7209^{+0.0065}_{-0.0065}$ ,  $b^2 = 0.0395^{+0.0080}_{-0.0080}$  and  $\zeta \leq 0.0173$  and for the third model  $\Omega_D = 0.7287^{+0.0062}_{-0.0062}$ ,  $b^2 = 0.0109^{+0.0023}_{-0.0023}$  and  $\zeta \leq 0.00764$ .

### 3. Non-linear interacting GGDE model in flat universe

As already mentioned, the main purpose of this paper is to examine the impact of non-linear interaction terms on the evolution of the universe. Beside to the notes mentioned in introduction, it has been shown in<sup>80</sup> that GGDE with specific non-linear interaction terms is a well behaved model and it shows a radiation dominated phase at the early times, passes through a matter dominated phase and finally ends in a stable dark energy dominated epoch. Moreover considering the non-linear terms, cure the linearly interacting GGDE which suffers from the absence of radiation dominated epoch in the early times evolution of the model.<sup>80</sup> In choosing the form of non-linear interaction terms, we follow the prescription presented in.<sup>67</sup> The closed form of the interaction which includes a large variety of choices is

$$Q = 3Hb^2 \rho_m^p \rho_D^s \rho^r, \quad (3.1)$$

where  $\rho = \rho_m + \rho_D$  and  $b^2$  is coupling constant factor also  $p$ ,  $s$  and  $r$  are integer numbers and one can deduce from the dimensional analysis that they should satisfy  $p+s+r = 1$ . In the following we choose three non-linear interactions and investigate their properties and features. In the selection of these interactions we have noted that the model should be cosmologically accepted which means that the dynamical equations must be smooth. For instance selecting the interaction terms with  $p = 0, s = 0, r = 1$  or  $p = 0, s = 2, r = -1$ , the dynamical equations of the model is singular and so the model is unphysical. It must point out that our assumption for functional form of interaction,  $Q$ , removes any degeneracy with modified Chaplygin gas model.

#### 3.1. Model I

In this model we consider following non-linear interaction form

$$Q = 3b^2 H \frac{\rho_D^3}{\rho^2}, \quad (3.2)$$

for this interaction, noticing (2.11) one finds that  $Q' = \frac{2b^2 \rho_D^2}{\rho^2}$  and considering the fact that  $\rho = \rho_m + \rho_D$ , it can be rewritten as  $Q' = 2b^2 \Omega_D^2$ . By inserting this relation to (2.11) and (2.13) we find

$$w_D = \frac{\zeta - \Omega_D - 2b^2 \Omega_D^3}{\Omega_D(2 - \Omega_D - \zeta)}, \quad (3.3)$$

$$q = \frac{1}{2} + \frac{3}{2} \frac{\zeta - \Omega_D - 2b^2 \Omega_D^3}{2 - \zeta - \Omega_D}. \quad (3.4)$$

It turns out that the above relations reduce to the corresponding expressions of non-interacting model (2.16) when  $b = 0$ . In Fig.(1) we have depicted the evolution of  $w_D$  as a function of scale factor for various values of the free parameters for this model. It is also clear from Fig. (1) that at late time, for some values of the free parameters, we get  $w_D < -1$ , which show a phantom like behavior of this interacting



Consistency of Nonlinearly Interacting Ghost Dark Energy with Recent Observations 9

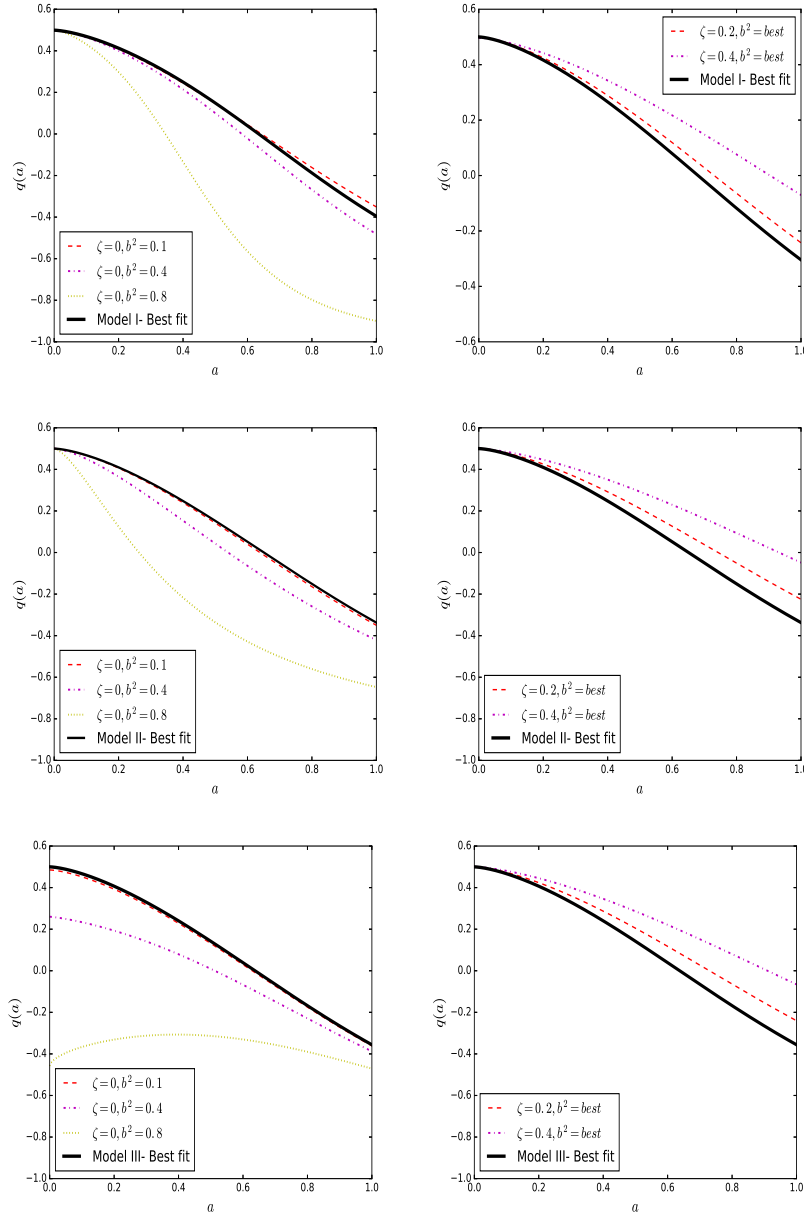


Fig. 2. The evolution of  $q$  as a function of scale factor for three models explained in the text. The rest information is the same as that of mentioned in Fig. 1.

GGDE model. Fig. (2) indicates the deceleration parameter as a function of scale factor for various choices of  $\zeta$  and  $b^2$  parameters. Increasing the value of  $b^2$  causes

10 *E. Ebrahimi, H. Golchin, A. Mehrabi, S. M. S. Movahed*

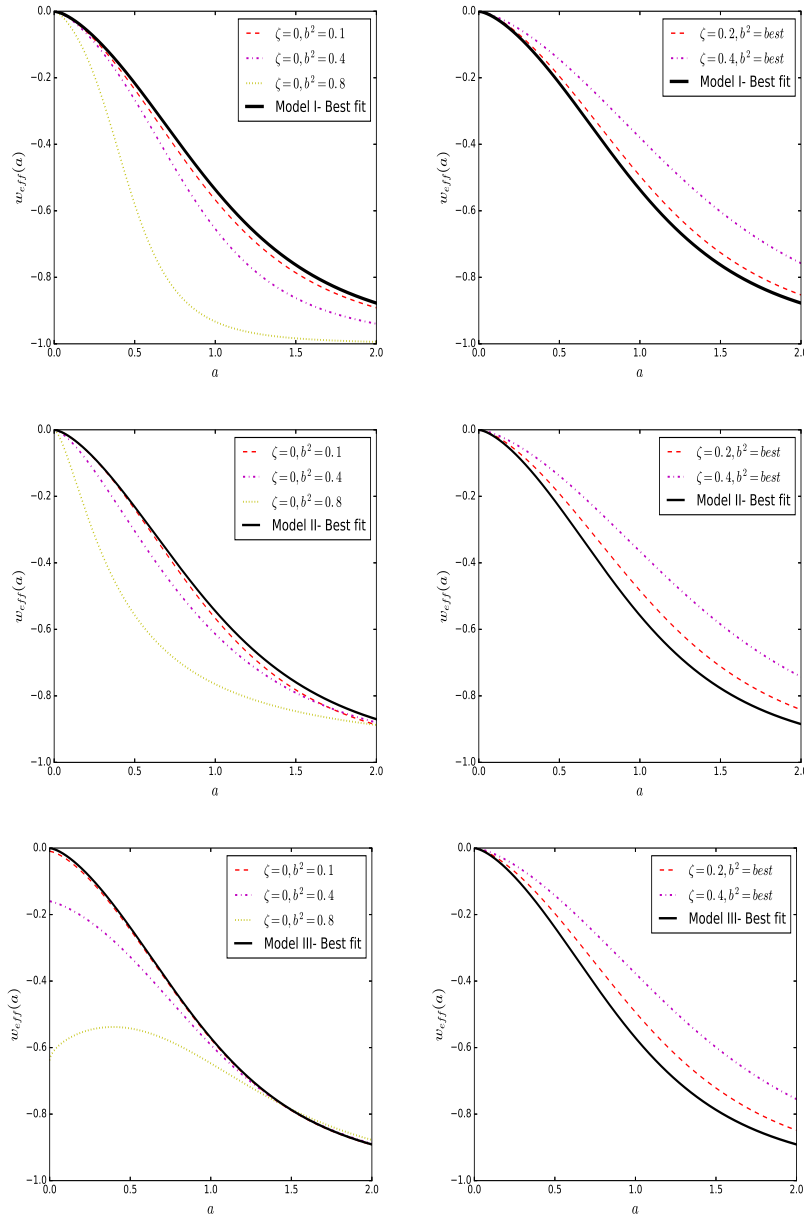


Fig. 3. The evolution of  $w_{eff}$  as a function of scale factor for three models explained in the text. The rest information is the same as that of mentioned in Fig. 1.

to decreasing  $q$  and getting the negative value at earlier time while according to right panel of Fig.(2), higher values of  $\zeta$  resulting the higher values of decelerating

parameter. In order to discuss about the fate of the universe filled with DM and GGDE components we should consider the effective equation of state parameter:

$$w_{eff} = \frac{P}{\rho}. \quad (3.5)$$

Taking  $P_m = 0$ , it can be found that  $w_{eff} = \Omega_D w_D$ . Fig.(3) represents  $w_{eff}$  as a function of scale factor. Our results demonstrate that  $w_{eff} \rightarrow -1$  at future implying that the universe will end with a big rip. It can be seen from Fig.(3) that the universe enters a acceleration phase earlier for larger values of  $b$ . In this case the evolution of DE density parameter can be computed using (2.14), the result is

$$\frac{d\Omega_D}{d \ln a} = \frac{3(\zeta - \Omega_D)(-1 + \Omega_D + b^2 \Omega_D^3)}{2 - \Omega_D - \zeta}. \quad (3.6)$$

The evolution of DE density parameter versus  $a$  is depicted in Fig.(4). In the left part of this figure, we turned to the impact of the coupling constant  $b$  on the density parameter evolution. This figure shows that for larger values of  $b$  the evolution of  $\Omega_D$  will be flatter. In the right panel of Fig.(4), evolution of  $\Omega_D$  is plotted for different choices of  $\zeta$  and best value for  $b^2$  (see next section). This figure reveals that the main advantages of the squared term in the dark energy density happens in early stages of the universe. This result was expected because the second order term is very small at late epochs (due to smallness of  $H$  at late time ). So it seems that the second term just can affect the late time acceleration problem through its primary effects on the cosmic dynamics in earlier stages.

Currently our universe is in dark energy dominated phase, so any successful model must be able to result in a late time stable universe in the dark energy dominated phase. In order to consider the stability issue of a dark energy model we should discuss a covariant perturbation theory in an expanding background. However in this step we do not follow such a process. In fact, here we are interested to do a simple analysis to see if the universe shows signs of stability in the DE dominated phase.

To this end we consider the response of the cosmic background filled with GDE and DM to adiabatic perturbations in linear regime. The governing equation on the evolution of the universe in this analysis includes continuity, Euler and Poisson equations. Inserting a small perturbation in energy density of the background and obtaining the resulting equations on evolution of the perturbations up to the first order one finds

$$\ddot{\delta} + 2H\dot{\delta} + v_s^2 k^2 \delta - 4\pi G \delta \rho_0 = 0, \quad (3.7)$$

where  $\delta$  is energy density perturbation of the fluid. For short wavelength the solution of above equation are of the form  $\delta \propto e^{\pm i\omega t}$ , where  $\omega \propto v_s$ . Now it is clear that when  $v_s^2 < 0$ , the perturbations can grow and makes the background unstable while for  $v_s^2 > 0$  the perturbations propagate oscillatory and the background will be stable against linear adiabatic perturbations. The way we use squared sound speed here

is that we search for epochs with positive  $v_s^2$  because we need a late time stable DE dominated universe. Here we look for impacts of the non-linear interaction terms to see if it leaves any chance for a late time positive  $v_s^2 > 0$ . Using

$$v_s^2 = \frac{dp}{d\rho} = \frac{\dot{p}}{\dot{\rho}}, \quad (3.8)$$

and taking into account the cosmic dynamic equations with non-linear interactions, after a little algebra one can find the squared sound speed as

$$v_s^2 = \frac{(\Omega_D - 1)(\Omega_D - \zeta)}{(\Omega_D - 2 + \zeta)^2} + \frac{\Omega_D^2(\Omega_D \zeta + 2\Omega_D - 6\zeta + 3\zeta^2)}{(\Omega_D - 2 + \zeta)^2} b^2. \quad (3.9)$$

In Fig.(5),  $v_s^2$  is drawn versus  $a$ . From the left part it is obvious that for this class of interaction,  $v_s^2$  with suitable choice of coupling constant  $b$ , is capable to get positive values at the late times and this leaves a chance for stable dark energy dominated universe which favored by observations. Fig.(5) also indicates that for larger values of  $b$ ,  $v_s^2$  will transits earlier to positive domain. It is worth mentioning that GDE in non-interacting and linearly interacting cases suffers from the negativity of  $v_s^2$  at the late times<sup>79</sup> and this is a direct consequence of this form of non-linear interaction term. The right part of Fig.(5) reveals that for larger values of  $\zeta$ ,  $v_s^2$  will enter to the positive domain later.

The evolution of scale factor as a function of time can be computed using Eq. (2.9) as follows:

$$\int_{a_0}^a (\Omega_D - \zeta) \frac{da'}{a'} = \int_{t_0}^t \frac{8\pi G\alpha}{3} dt' = B(t - t_0) \quad (3.10)$$

where  $B \equiv \frac{8\pi G\alpha}{3}$ . Fig. (6) illustrates the behavior of scale factor as a function of time.

### 3.2. Model II

In this model we consider the following form for non-linear interaction term

$$Q = 3b^2 H \frac{\rho_D \rho_m}{\rho}. \quad (3.11)$$

In this case, one finds that  $Q' = \frac{2b^2 \rho_m}{\rho} = 2b^2 \Omega_m$  consequently, we can rewrite the equation of state and deceleration parameters as

$$w_D = \frac{\zeta - \Omega_D - 2b^2 \Omega_D (1 - \Omega_D)}{\Omega_D (2 - \Omega_D - \zeta)}, \quad (3.12)$$

$$q = \frac{1}{2} + \frac{3}{2} \frac{\zeta - \Omega_D - 2b^2 \Omega_D (1 - \Omega_D)}{2 - \zeta - \Omega_D}. \quad (3.13)$$

It is easy to see that these relations in the late and early time limits approach to the non-interacting case, however they differ from non-interacting case in middle stages of evolution. It is also worth to mention that in this case the phantom divide

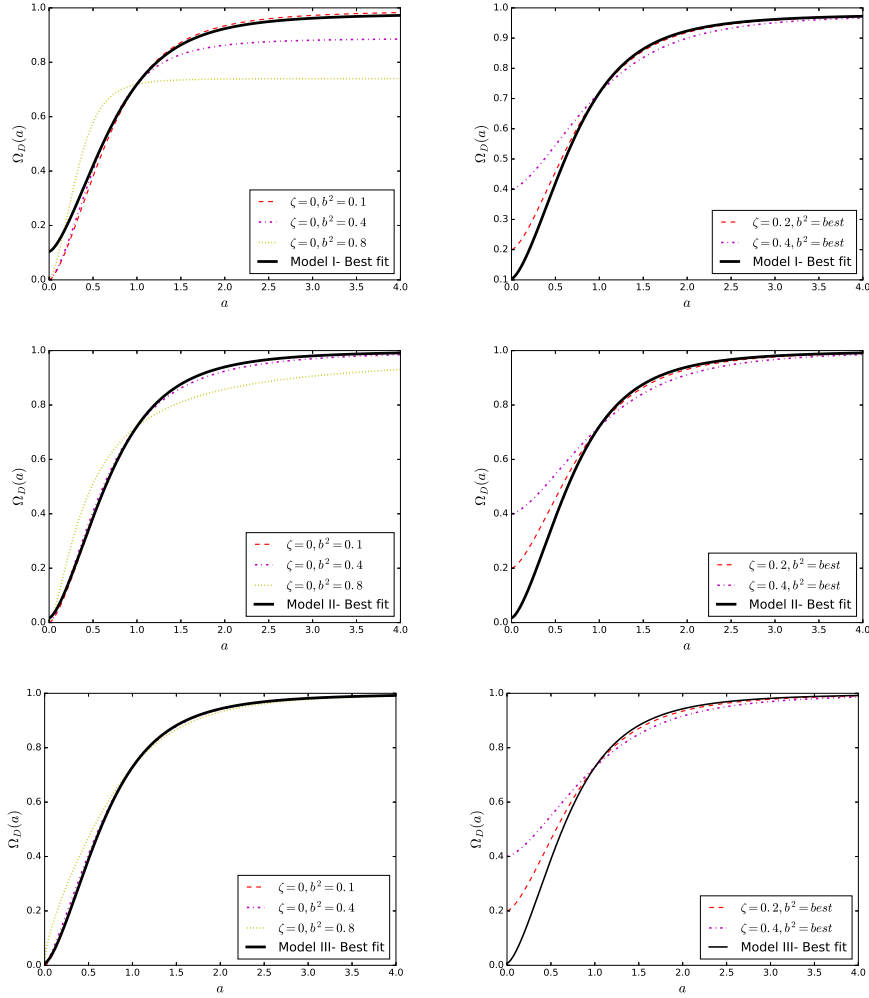


Fig. 4. The evolution of  $\Omega_D$  as a function of scale factor for three models explained in the text. The rest information is the same as that of mentioned in Fig. 1.

can not be crossed. To make more obvious the mentioned behavior, we have plotted the relevant parameters.

In Fig.(1) we found that the evolution of  $w_D$  versus scale factor. Fig.(2) indicates the deceleration parameter as function of scale factor for various choices of  $\zeta$  and  $b^2$  parameters. Increasing the value of  $b^2$  causes to decreasing  $q$  and getting the negative value at earlier times while according to the right panel of Fig.(2), larger values of  $\zeta$  leads to the larger deceleration parameters. Note that to ensure  $q < 0$  at the present time ( $a = 1$ ), we should set  $\zeta < 0.4$ . This theoretical constraint is consistent to the other observational constraints (the next section).

14 *E. Ebrahimi, H. Golchin, A. Mehrabi, S. M. S. Movahed*

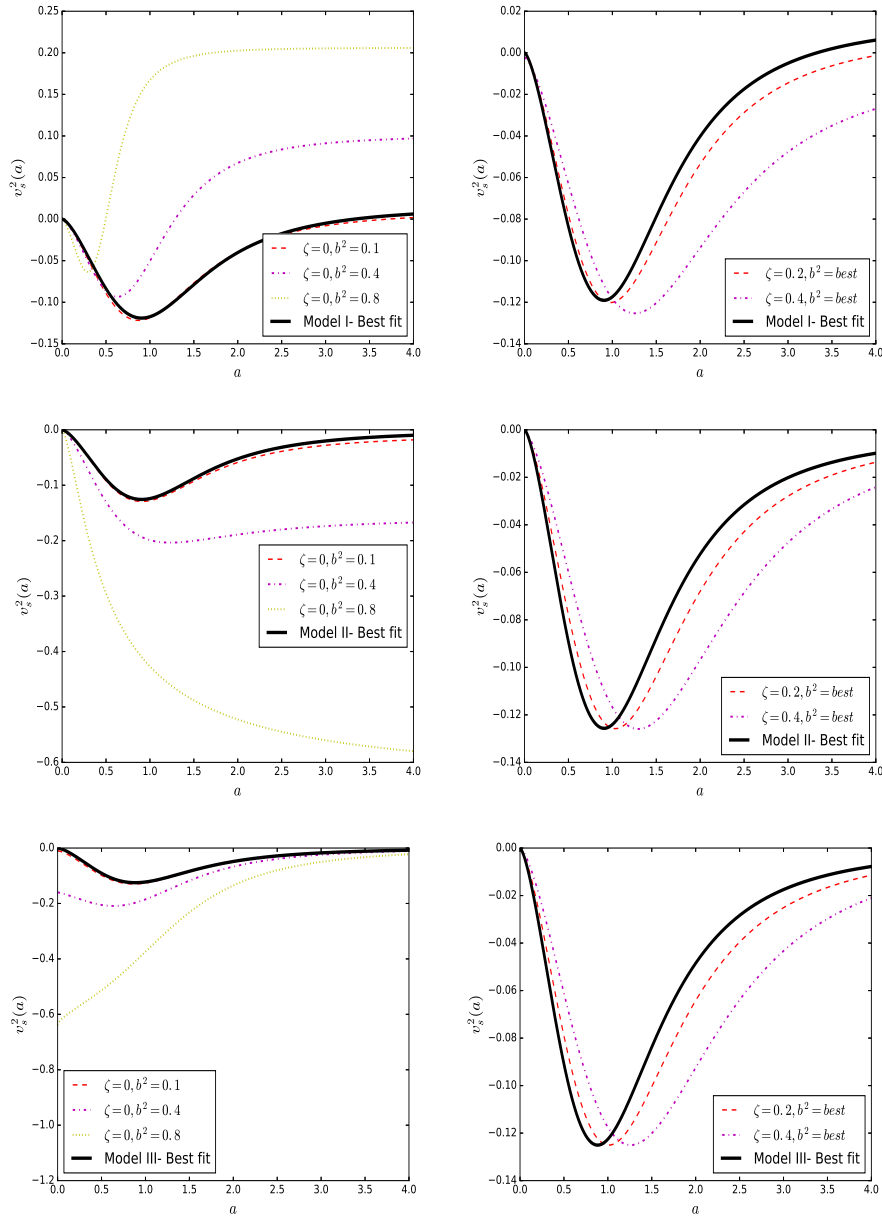


Fig. 5. The evolution of  $v_s^2$  as a function of scale factor for three models explained in the text. The rest information is the same as that of mentioned in Fig. 1.

Fig.(3) illustrates  $w_{eff}$  as a function of scale factor. Our results demonstrate that  $w_{eff} \rightarrow -1$  at future implying that the universe will end with a big rip as the

previous case. It can be seen from Fig.(3) that  $w_{eff}$  gets more negative values by increasing the coupling  $b^2$ . One can also find the evolution of DE density parameter for this case as

$$\frac{d\Omega_D}{d \ln a} = \frac{3(\zeta - \Omega_D)(1 - \Omega_D)(b^2\Omega_D - 1)}{2 - \Omega_D - \zeta}. \quad (3.14)$$

The left part of Fig.(4) corresponds to the impact of the coupling constant  $b^2$  on the density parameter evolution. This figure shows that larger values of  $b^2$ , extend the dominant era of  $\Omega_D$ . In right panel of this figure, the evolution of  $\Omega_D$  is plotted for different choices of  $\zeta$ .

In this case the squared sound speed can be obtained as:

$$v_s^2 = \frac{(\Omega_D - 1)(\Omega_D - \zeta)}{(\Omega_D - 2 + \zeta)^2} - \frac{\Omega_D^3 + (\zeta - 2)\Omega_D^2 + (2\zeta^2 - 5\zeta + 2)\Omega_D - \zeta^2 + 2\zeta}{(\Omega_D - 2 + \zeta)^2} b^2. \quad (3.15)$$

Plotting  $v_s^2$  versus  $a$  in Fig.(5) reveals that the squared sound speed is always negative for different choices of constants implying that in present case, a late time stable GGDE dominated phase is a matter of doubt. It is also easy to see that by increasing  $b$ , the squared sound speed takes more negative values in contrast with the previous case.

### 3.3. Model III

The functional form of non-linear interaction for this model is considered as

$$Q = 3b^2 H \frac{\rho_m^2}{\rho}. \quad (3.16)$$

Doing the same steps for this interaction, one finds that  $Q' = 2b^2 \frac{\rho_m^2}{\rho \rho_D} = 2b^2 \frac{\Omega_m^2}{\Omega_D}$ , and the EoS and deceleration parameters as

$$w_D = \frac{\zeta - \Omega_D - 2b^2(1 - \Omega_D)^2}{\Omega_D(2 - \Omega_D - \zeta)} \quad (3.17)$$

$$q = \frac{1}{2} + \frac{3}{2} \frac{\zeta - \Omega_D - 2b^2(1 - \Omega_D)^2}{2 - \zeta - \Omega_D}. \quad (3.18)$$

In this case the dark energy density parameter evolves as

$$\frac{d\Omega_D}{d \ln a} = \frac{3(\zeta - \Omega_D)(\Omega_D - 1)(b^2\Omega_D + 1 - b^2)}{2 - \Omega_D - \zeta}. \quad (3.19)$$

The behavior of equation of state,  $w_D$ , deceleration parameter,  $q$ , effective equation of state,  $w_{eff}$  and energy density of DE have been plotted in Figs. (1), (2), (3) and (4), respectively. Finally the squared sound speed for this case reads

$$v_s^2 = \frac{(\Omega_D - 1)(\Omega_D - \zeta)}{(\Omega_D - 2 + \zeta)^2} + \frac{(\Omega_D - 1) [\Omega_D^2 + (\zeta - 3)\Omega_D + (2\zeta - 5)\zeta + 4]}{(\Omega_D - 2 + \zeta)^2} b^2. \quad (3.20)$$

Fig.(5) shows that in this case  $v_s^2$  can not get positive values but approaches the border line at the future. The model with smaller value of  $b$  will approaches the

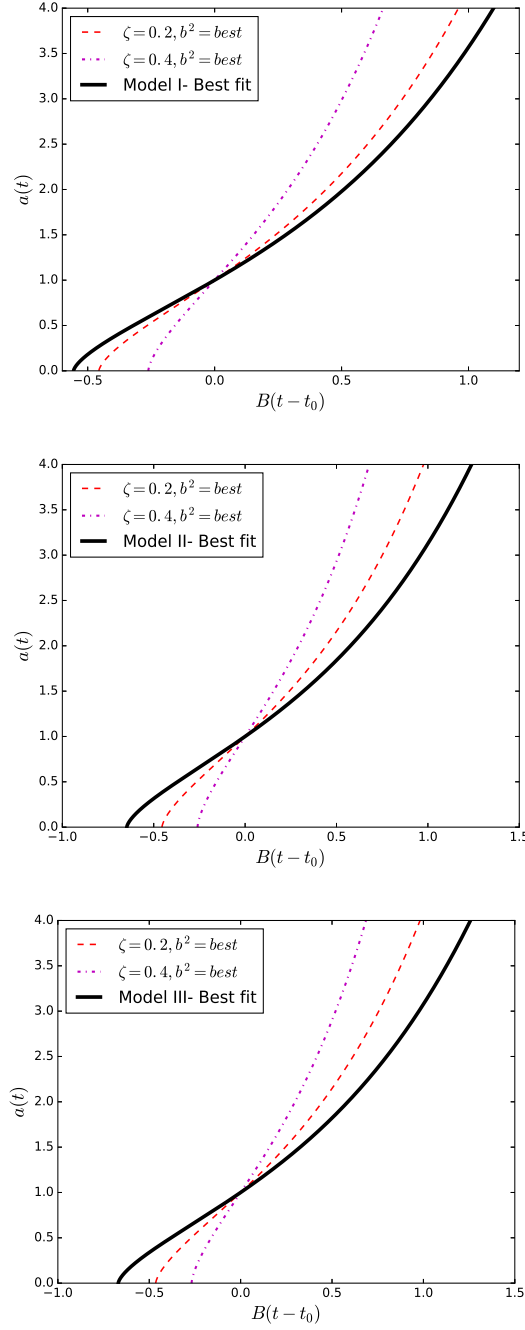


Fig. 6. The evolution of scale factor as a function of time. Here  $B \equiv \frac{8\pi G\alpha}{3}$ , the value of  $\Omega_D$  at the present time and  $b^2$  have been fixed according to their best values determined by joint analysis of SNIa+Hubble+BAO+CMB. In all plots the dark solid line corresponds to the best fit values determined by joint analysis.



border line earlier. Finally, the behavior of scale factor as a function of time is represented in Fig.(6). This plot shows that the model in principle, can explain the late accelerating expansion of the universe. In the next section we are going to carry out the comparison between results given by our models and that of given directly from observation.

#### 4. Observational consistency check

In this section, we rely on the most recent observational data sets to check the consistency of generalized ghost dark energy model accompanied by non-linear interactions between DM and DE. This approach enables us to put observational constraints on the free parameters of our model and asses how the presence of interaction is suitable as an alternative paradigm. The following observables for examination of the nature of dark energy can be used:

- I) Expansion history of the Universe
- II) Changing the evolution of gravitational potentials, causing to ISW effect
- III) Cross-correlation of CMB and large scale structures
- IV) Growth of structures
- V) Weak lensing

In this paper we limit ourselves on almost evolution expansion indicators such as distance modulus of Supernovae Type Ia and the Hubble parameter, Baryon acoustic oscillations (BAO) and CMB including the position of first peak, shift parameter and redshift of recombination. Throughout this paper we have supposed that our Universe is flat, so  $\Omega_{tot} = \Omega_m + \Omega_b + \Omega_r + \Omega_D = 1$ , where  $\Omega_m, \Omega_b$  denote the density parameters of dark matter and baryonic matter respectively. Energy density of radiation and baryonic matter are fixed by other relevant observations. For more convenience, we indicate free parameters by  $\Theta : \{\Omega_D, \zeta, b^2\}$ . The expected priors on these parameters are listed in Table 1. Radiation density is fixed to  $\Omega_r = 2.469 \times 10^{-5} h^{-2} (1.6903)$ .<sup>81</sup> The baryonic density is set to  $\Omega_b h^2 = 0.02222 \pm 0.00023$ <sup>82</sup>

Table 1. Priors on free parameter space, used in the observational constraints analysis in this paper.

Parameter	Prior	Shape of PDF
$\Omega_{tot}$	1.000	Fixed
$\zeta$	[0.050 – 0.020]	Top-Hat
$H_0$	[40.0 – 100.0]	Top-Hat
$\Omega_D$	[0.0 – 1.0]	Top-Hat
$b^2$	[0.0 – 1.0]	Top-Hat

#### 4.1. *Supernovae Ia*

In order to compute cosmological distance, we must look for standard candles. Such brilliant cosmological objects enable us to determine cosmological distance for a given redshift corresponding to mentioned object. Type Ia supernovae is a category of cataclysmic variable stars produced due to explosion of a white dwarf star. Its thermonuclear explosion is well known, consequently, it can be used as standard candle. In 1998, Riess et al., could discover the acceleration of expanding universe using 16 distant and 34 nearby SNIa from the Hubble space telescope (HST) project.<sup>1</sup> After that, Perlmutter et al., using SNIa from Calan-Tololo and 42 high-redshift SN, confirmed acceleration expansion.<sup>2</sup> The surveys of SNIa have drawn more attention. Higher-Z Team,<sup>83,84</sup> the Supernova Legacy Survey (SNLS),<sup>85–88</sup> the ESSENCE,<sup>89,90</sup> the Nearby Supernova Factory (NSF),<sup>91,92</sup> the Carnegie Supernova Project (CSP),<sup>93,94</sup> the Lick Observatory Supernova Search (LOSS),<sup>95,96</sup> the Sloan Digital Sky Survey (SDSS) SN Survey,<sup>97,98</sup> Union2.1 SNIa dataset.<sup>99,100</sup> More recently a catalog made from SNLS and SDSS SNIa compilation which is called Joint Light-curve Analysis (JLA) was produced.<sup>101</sup> In this paper we consider constraints on model parameters coming from SNIa observations using JLA dataset including 740 Ia supernovae in the redshift range of  $z \in [0.01, 1.30]$ .<sup>101</sup>

Observation of SNIa does not provide standard ruler but rather gives distance modulus. This quantity is defined by:

$$\mu(z; \{\Theta\}) \equiv m - M = 5 \log \left( \frac{d_L(z; \{\Theta\})}{\text{Mpc}} \right) + 25 \quad (4.1)$$

where  $m$  and  $M$  are apparent and absolute magnitude, respectively. For the spatially flat universe the luminosity distance defined in above equation reads as:

$$d_L(z) = \frac{c}{H_0} (1+z) \int_0^z \frac{dz'}{\mathcal{H}(z'; \{\Theta\})} \quad (4.2)$$

where  $\mathcal{H} = H/H_0$ . To compare the observational data and that determined by our model, we apply the likelihood analysis. To this end, we use  $\chi^2$  which is defined as

$$\chi_{SNIa}^2 \equiv \Delta\mu^\dagger \cdot \mathcal{C}_{SNIa}^{-1} \cdot \Delta\mu \quad (4.3)$$

where  $\Delta\mu \equiv \mu_{obs}(z) - \mu(z; \{\Theta\})$  and correlation information of SNIa data sets is encoded in covariance matrix,  $\mathcal{C}_{SNIa}$ . The observed distance moduli and the relevant covariance matrix can be found on the web site.<sup>102,103</sup> Here  $\mu_{obs}(z)$  is observed distance modulus for a SNIa located at redshift  $z$ . Marginalizing over  $H_0$  as a nuisance parameter yields<sup>8,104</sup>

$$\chi_{SNIa}^2 = \mathcal{M}^\dagger \cdot \mathcal{C}_{SNIa}^{-1} \cdot \mathcal{M} + \mathcal{A}_{SNIa} + \mathcal{B}_{SNIa} \quad (4.4)$$

where  $\mathcal{M}(z) \equiv \mu_{obs}(z) - 25 - 5 \log_{10}[H_0 d_L(z; \{\Theta\})/c]$ , and

$$\mathcal{A}_{SNIa} \equiv - \frac{\left[ \sum_{i,j} \mathcal{M}(z_i) \mathcal{C}_{SNIa}^{-1}(z_i, z_j) - \ln 10/5 \right]^2}{\sum_{i,j} \mathcal{C}_{SNIa}^{-1}(z_i, z_j)} \quad (4.5)$$

$$\mathcal{B}_{SNIa} \equiv -2 \ln \left( \frac{\ln 10}{5} \sqrt{\frac{2\pi}{\sum_{i,j} \mathcal{C}_{SNIa}^{-1}(z_i, z_j)}} \right) \quad (4.6)$$

#### 4.2. OHD dataset

In addition to SNIa standard candles, we use Observational Hubble parameter Data (OHD).<sup>105</sup> In this case the chi-square is:

$$\chi_H^2 = \sum_i \frac{[H_{obs}(z_i) - H(z_i, \{\Theta\})]^2}{\sigma^2(z_i)} \quad (4.7)$$

where  $H_{obs}$  is observed Hubble parameter and  $H$  is given by Eq. (2.1).

#### 4.3. Baryon acoustic oscillations

The footprint of oscillations in the baryon-photon plasma on the matter power spectrum is recognized by Baryon Acoustic Oscillation (BAO). The acoustic scale is so large therefore BAO are largely unaffected by nonlinear evolution. Usually, the BAO data is applied to measure both the angular diameter distance  $D_A(z; \{\Theta\})$ , and the expansion rate of the Universe  $H(z; \{\Theta\})$ :<sup>8</sup>

$$D_V(z; \{\Theta\}) = \left[ (1+z)^2 D_A^2(z; \{\Theta\}) \frac{cz}{H(z; \{\Theta\})} \right]^{1/3} \quad (4.8)$$

where  $D_V(z; \{\Theta\})$  is volume-distance. The distance ratio is defined by

$$d(z; \{\Theta\}) \equiv \frac{r_s(z; \{\Theta\})}{D_V(z; \{\Theta\})} \quad (4.9)$$

here  $r_s(z; \{\Theta\})$  is the comoving sound horizon. In order to take into account various aspects of BAO observations, we use six BAO indicators including Sloan Digital Sky Survey (SDSS) data release 7 (DR7),<sup>106</sup> SDSS-III Baryon Oscillation Spectroscopic Survey (BOSS),<sup>107</sup> WiggleZ survey<sup>108</sup> and 6dFGS survey.<sup>109</sup> These measurements include redshifts in the range  $z \in [0.1, 0.7]$ . Table 2 reports the observed value of mentioned parameters.

The fisher information matrix is given by<sup>81</sup>

$$\mathcal{C}_{BAO}^{-1} = \begin{pmatrix} 4444.4 & 0 & 0 & 0 & 0 & 0 \\ 0 & 34.602 & 0 & 0 & 0 & 0 \\ 0 & 0 & 20.661157 & 0 & 0 & 0 \\ 0 & 0 & 0 & 24532.1 & -25137.7 & 12099.1 \\ 0 & 0 & 0 & -25137.7 & 134598.4 & -64783.9 \\ 0 & 0 & 0 & 12099.1 & -64783.9 & 128837.6 \end{pmatrix}. \quad (4.10)$$

20 *E. Ebrahimi, H. Golchin, A. Mehrabi, S. M. S. Movahed*

Table 2. Observed data for BAO.<sup>81</sup>

Redshift	Data Set	$r_s/D_V(z; \{\Theta\})$	Ref.
0.10	6dFGS	$0.336 \pm 0.015$	<sup>109</sup>
0.35	SDSS-DR7-rec	$0.113 \pm 0.002$	<sup>106</sup>
0.57	SDSS-DR9-rec	$0.073 \pm 0.001$	<sup>107</sup>
0.44	WiggleZ	$0.0916 \pm 0.0071$	<sup>110</sup>
0.60	WiggleZ	$0.0726 \pm 0.0034$	<sup>110</sup>
0.73	WiggleZ	$0.0592 \pm 0.0032$	<sup>110</sup>

Accordingly,  $\chi_{BAO}^2$  is written by

$$\chi_{BAO}^2 \equiv \Delta d^\dagger \cdot C_{BAO}^{-1} \cdot \Delta d. \quad (4.11)$$

In above equation  $\Delta d(z; \{\Theta\}) \equiv d_{obs}(z) - d(z; \{\Theta\})$ , where  $C_{BAO}^{-1}$  is given in (4.10) and  $d_{obs}(z)$  is reported in table 2. In the next subsection for sake of clarity, we will give proper explanation about the main constraints with CMB observations mainly affecting the background evolution.

#### 4.4. CMB observations

The most popular quantities devoted to CMB power spectrum are the position of sound horizon in power spectrum ( $l_a$ ), CMB shift parameter ( $R$ ) and the redshift of recombination ( $z_*$ ). The sound horizon angular scale at recombination in the flat Universe read as

$$l_a = \pi \frac{\int_0^{z_*} \frac{dz}{H(z; \{\Theta\})}}{r_s(z_*; \{\Theta\})}. \quad (4.12)$$

The CMB shift parameter represented by  $R$  is defined by

$$R(z_*; \{\Theta\}) = \sqrt{\Omega_m} \int_0^{z_*} \frac{dz}{\mathcal{H}(z; \{\Theta\})}. \quad (4.13)$$

here, the redshift at the recombination expresses as  $z_* = 1048[1 + 0.00124(\Omega_b h^2)^{-0.738}(1 + g_1(\Omega_m h^2)^{g_2})]$ . Where the relevant parameters  $g_1$  and  $g_2$  can be found in Ref.<sup>111</sup>

$$g_1 = \frac{0.0783 (\Omega_b h^2)^{-0.238}}{1 + 39.5 (\Omega_b h^2)^{0.763}}, \quad (4.14)$$

$$g_2 = \frac{0.560}{1 + 21.1 (\Omega_b h^2)^{1.81}}. \quad (4.15)$$

To consider the contribution of mentioned observational quantities, we use following likelihood function for CMB observation:<sup>81</sup>

$$\chi_{CMB}^2 = \Delta \mathcal{D}^\dagger \cdot C_{CMB}^{-1} \cdot \Delta \mathcal{D}, \quad (4.16)$$

where  $\Delta\mathcal{D} \equiv \mathcal{D}_{obs} - \mathcal{D}(\{\Theta\})$ , in which  $\mathcal{D}_{obs}$  for the 9-year WMAP (WMAP9) observation with flat prior are<sup>81</sup>

$$\mathcal{D}_{obs} \equiv \begin{pmatrix} l_a \\ R \\ z_*$$

and  $\mathcal{C}_{CMB}$  is as follows

$$\mathcal{C}_{CMB}^{-1} = \begin{pmatrix} 3.182 & 18.253 & -1.429 \\ 18.253 & 11887.879 & -193.808 \\ -1.429 & -193.808 & 4.556 \end{pmatrix}. \quad (4.18)$$

According to Planck TT+LowP data the most important parameters to use are<sup>8</sup>

$$\mathcal{D}_{obs} \equiv \begin{pmatrix} l_a \\ R \\ \Omega_b h^2 \end{pmatrix} = \begin{pmatrix} 301.76, \\ 1.7488 \\ 0.02228 \end{pmatrix}, \quad (4.19)$$

and  $\mathcal{C}_{CMB}$  is as follows

$$\mathcal{C}_{CMB} = \begin{pmatrix} 1 & 0.54 & -0.63 \\ 0.54 & 1 & -0.43 \\ -0.63 & -0.43 & 1 \end{pmatrix}. \quad (4.20)$$

In this paper we use the former observational quantities for CMB. Finally, we perform a MCMC analysis using joint likelihood of both standard rulers and standard candles. The combined chi-square function is:

$$\chi_{SHBC}^2 = \chi_{Sn}^2 + \chi_H^2 + \chi_{BAO}^2 + \chi_{CMB}^2. \quad (4.21)$$

The abbreviation (SHBC) stands in above equation is replaced by SNIa+Hubble+BAO+CMb. In the next subsection we will summarize the results achieved for best fit values of the free parameters and compare them.

#### 4.5. Results

In the following, we present the observational constraints on the free parameters of ghost dark energy model with three interaction terms introduced in section 3.

**Model I:**  $Q = 3b^2 H \frac{\rho_\phi^3}{\rho^2}$

SNIa observational constraint shows that  $\Omega_D = 0.753_{-0.060}^{+0.038}$ ,  $\zeta = 0.23_{-0.15}^{+0.12}$  and  $b^2 = 0.23_{-0.18}^{+0.10}$  at  $1\sigma$  confidence interval. The best fit values at 68% and 95% intervals for SNIa using JLA catalog are reported in Table 3. Combining the other observational data sets, namely Hubble parameters, BAO and CMB with SNIa observation results in  $\Omega_D = 0.7192_{-0.0062}^{+0.0062}$ ,  $\zeta = 0.104_{-0.047}^{+0.047}$  and  $b^2 = 0.146_{-0.026}^{+0.030}$  at  $1\sigma$  confidence interval. Table 3 reports the value at 68% and 95% optimal variance errors. Upper left panels of Fig. 7 illustrates the marginalized likelihood functions and contours

22 *E. Ebrahimi, H. Golchin, A. Mehrabi, S. M. S. Movahed*

Table 3. Best fit values for non-linear interacting dark energy model I using SNIa, SNIa+Hubble+BAO and joint combination of SNIa+Hubble+BAO+CMB (SHBC) at 68% and 95% confidence intervals.

Parameters of model I	SNIa	SNIa+Hubble+BAO	SHBC
$\Omega_D$	$0.753^{+0.038+0.094}_{-0.060-0.081}$	$0.722^{+0.026+0.060}_{-0.036-0.054}$	$0.7192^{+0.0062+0.012}_{-0.0062-0.012}$
$\zeta$	$0.23^{+0.12+0.20}_{-0.15-0.23}$	$0.161 \pm 0.084 < 0.304$	$0.104^{+0.047+0.085}_{-0.047-0.096}$
$b^2$	$0.23^{+0.10}_{-0.18} < 0.443$	$0.28^{+0.11+0.19}_{-0.11-0.19}$	$0.146^{+0.030+0.050}_{-0.026-0.057}$

Table 4. Best fit values for non-linear interacting dark energy model II using SNIa, SNIa+Hubble+BAO and joint combination of SNIa+Hubble+BAO+CMB (SHBC) at 68% and 95% confidence intervals.

Parameter of model II	SNIa	SNIa+Hubble+BAO	SHBC
$\Omega_D$	$0.779^{+0.054+0.088}_{-0.046-0.096}$	$0.796^{+0.029+0.052}_{-0.021-0.055}$	$0.7209^{+0.0065+0.0130}_{-0.0065-0.0130}$
$\zeta$	$0.22^{+0.10}_{-0.16} < 0.430$	$< 0.154 < 0.285$	$< 0.0173 < 0.0373$
$b^2$	$0.27^{+0.15+0.21}_{-0.12-0.23}$	$< 0.0669 < 0.1420$	$0.0395^{+0.0080+0.0160}_{-0.0080-0.0150}$

Table 5. Best fit values for non-linear interacting dark energy model III using SNIa, SNIa+Hubble+BAO and joint combination of SNIa+Hubble+BAO+CMB (SHBC) at 68% and 95% confidence intervals.

Parameter of model III	SNIa	SNIa+Hubble+BAO	SHBC
$\Omega_D$	$0.831^{+0.038+0.064}_{-0.032-0.066}$	$0.814^{+0.020+0.046}_{-0.024-0.040}$	$0.7287^{+0.0062+0.0120}_{-0.0062-0.0120}$
$\zeta$	$0.216^{+0.099}_{-0.160} < 0.424$	$0.150^{+0.054}_{-0.130} < 0.325$	$< 0.00764 < 0.0173$
$b^2$	$0.28^{+0.15+0.20}_{-0.11-0.24}$	$< 0.0433 < 0.0897$	$0.0109^{+0.0023+0.0044}_{-0.0023-0.0045}$

for free parameter of first dark energy model using SNIa, SNIa+Hubble+BAO and SNIa+Hubble+BAO+CMB respectively.

**Model II:**  $Q = 3b^2 H \frac{\rho_D \rho_m}{\rho}$ 

For this model, SNIa observations constrain the value of parameters as:  $\Omega_D = 0.779^{+0.054}_{-0.046}$ ,  $\zeta = 0.22^{+0.10}_{-0.16}$  and  $b^2 = 0.27^{+0.15}_{-0.12}$  at  $1\sigma$  confidence interval. The best fit values at 68% and 95% intervals for SNIa and their joint analysis are reported in table 4. Combining Hubble parameters, BAO and CMB observational data sets with SNIa, results in  $\Omega_D = 0.7209^{+0.0065}_{-0.0065}$ ,  $\zeta < 0.0173$  and  $b^2 = 0.0395^{+0.0080}_{-0.0080}$  at  $1\sigma$  confidence interval. Table 4 reports the value at 68% and 95% levels. Upper right panels of Fig. 7 illustrate the marginalized likelihood functions and contours for free parameters of the second dark energy model.

**Model III:**  $Q = 3b^2 H \frac{\rho_m^2}{\rho}$ 

For the third interacting dark energy model, SNIa observations confine the value of parameters as:  $\Omega_D = 0.831^{+0.038}_{-0.032}$ ,  $\zeta = 0.216^{+0.099}_{-0.160}$  and  $b^2 = 0.28^{+0.15}_{-0.11}$  at  $1\sigma$  confidence interval. The best fit values at 68% and 95% intervals for SNIa and their joint analysis are reported in table 5. Combining the other observational data sets, namely Hubble parameters, BAO and CMB with SNIa observations leads to  $\Omega_D = 0.7287^{+0.0062}_{-0.0062}$ ,  $\zeta < 0.00764$  and  $b^2 = 0.0109^{+0.0023}_{-0.0023}$  at  $1\sigma$  confidence interval. Table 5 reports these values at 68% and 95% levels. Bottom panels of Fig. 7 illustrates the marginalized likelihood functions and contours for free parameters of this model.

In order to give a quantitative and robust measure to compare three interacting dark energy models with  $\Lambda$ CDM model as a reference model, we must go beyond computing  $\chi^2$  and take into account the number of degrees of freedom (dof). Referring to the fact that higher degrees of freedom usually cause to more consistency of the model and observations, we use AIC<sup>112</sup> and BIC<sup>113</sup> criteria. AIC is defined by:

$$\text{AIC} = -2 \ln \mathcal{L}_{\max} + 2g, \quad (4.22)$$

and BIC<sup>113</sup> is given by:

$$\text{BIC} = -2 \ln \mathcal{L}_{\max} + g \ln N, \quad (4.23)$$

In the above equations,  $g$  is the number of free parameters and  $N$  is the number of observational data sets used for constraining. The relative form of mentioned criteria are in principle utilized, namely  $\Delta\text{AIC} = \Delta\chi_{\min}^2 + 2\Delta g$  and  $\Delta\text{BIC} = \Delta\chi_{\min}^2 + \Delta g \ln N$ . The lower values of  $\Delta\text{AIC}$  and  $\Delta\text{BIC}$ , the more favored model by observational data sets. Regarding the capability of AIC and BIC measures, the former does not consider the number of observational data set, while the latter takes into accounts observations.<sup>114</sup> Since three models introduced in this paper have same degrees of freedom, therefore  $\Delta\text{AIC}$  and  $\Delta\text{BIC}$  don't make sense. Subsequently we compute  $\chi_{\min}^2$  for  $\Lambda$ CDM model considering two free parameters and suppose to be a reference model. In such case  $\Delta\text{AIC}$  less than 10 corresponds to consistent model with respect to the reference model. Our results demonstrate that our three interacting dark energy models are supported by observations, but they are worse than  $\Lambda$ CDM model but still are good models. If we consider only SNIa dataset, the corresponding  $\chi_{\min}^2$  for models are 682.247 for model I, 682.117 for model II, 682.057 for model III and 682.895 for  $\Lambda$ CDM. Therefore the value of

minimum  $\chi^2$  for all interacting dark energy models are smaller than  $\Lambda$ CDM due to their one more free parameter. If we take into account SNIa+Hubble+BAO the values of minimum chi-square are 705.537 for model I, 706.942 for model II, 707.122 for model III and 706.424 for  $\Lambda$ CDM. The relevant results for our three cases accompanying  $\Lambda$ CDM are summarized in Tabs.6, 7 and 8 . For SNIa observational constraint and its combination with Hubble+BAO, we find that all non-linear interacting dark energy models are relatively good models. While for SNIa+Hubble+BAO+CMB, all non-linear interacting models are worse than  $\Lambda$ CDM but they are relatively good models in the sense of declaring observations.

Table 6. The minimum value of  $\chi^2$ , AIC and BIC criteria for our models and  $\Lambda$ CDM when we use SNIa datasets.

Model	$\chi_{min}^2$	$\Delta$ AIC	$\Delta$ BIC	$\chi_{min}^2/\text{dof}$
$\Lambda$ CDM	682.895	0	0	0.925
I	682.247	1.352	5.959	0.926
II	682.117	1.222	5.829	0.925
III	682.057	1.162	5.769	0.925

Table 7. The minimum value of  $\chi^2$ , AIC and BIC criteria for our models and  $\Lambda$ CDM when we use SNIa+Hubble+BAO datasets.

Model	$\chi_{min}^2$	$\Delta$ AIC	$\Delta$ BIC	$\chi_{min}^2/\text{dof}$
$\Lambda$ CDM	706.424	0	0	0.908
I	705.537	1.113	5.772	0.908
II	706.942	2.518	7.177	0.910
III	707.122	2.698	7.357	0.910

Table 8. The minimum value of  $\chi^2$ , AIC and BIC criteria for our models and  $\Lambda$ CDM when we use SNIa+Hubble+BAO+CMB.

Model	$\chi_{min}^2$	$\Delta$ AIC	$\Delta$ BIC	$\chi_{min}^2/\text{dof}$
$\Lambda$ CDM	708.565	0	0	0.907
I	710.891	4.326	8.989	0.911
II	711.765	5.200	9.863	0.912
III	712.726	6.161	10.824	0.914

Finally, in order to compare three models of dark energy introduced in this paper, we indicate the behavior of  $\Omega_D$ ,  $q$ ,  $v_s^2$ ,  $w_d$  and  $w_{eff}$  for the best fit values of free parameters as a function of scale factor in Fig.8. As indicated in this plot, from the view point of  $q$  and  $w_{eff}$  the three models are rather similar and they show the expected behavior of accelerating expansion of the universe. There is also



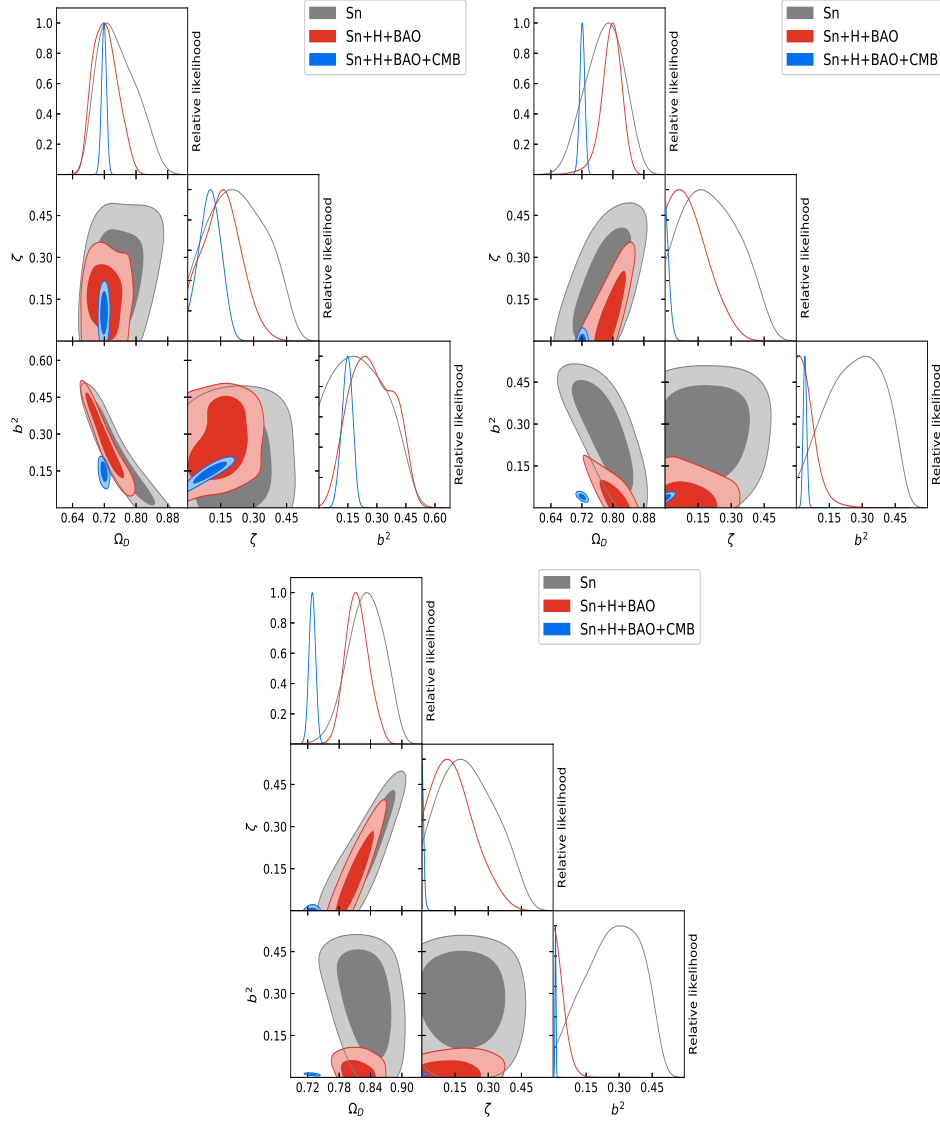


Fig. 7. Upper left panel corresponds to marginalized and contour plots of joint analysis base on SNIa, SNIa+Hubble+BAO and SNIa+Hubble+BAO+CMB observations. The upper right panel shows the same for second model while the lower panel is devoted to model III of non-linear interacting dark energy.

some features that distinct these models, for instance  $\Omega_D$  for model I takes non-zero value at very early universe while this quantity for model II and III goes to zero. The value of  $v_s^2$  for first model takes positive value for  $a > 1$  but for second and third models this quantity always remains in the negative domain. The  $w_D$  for third

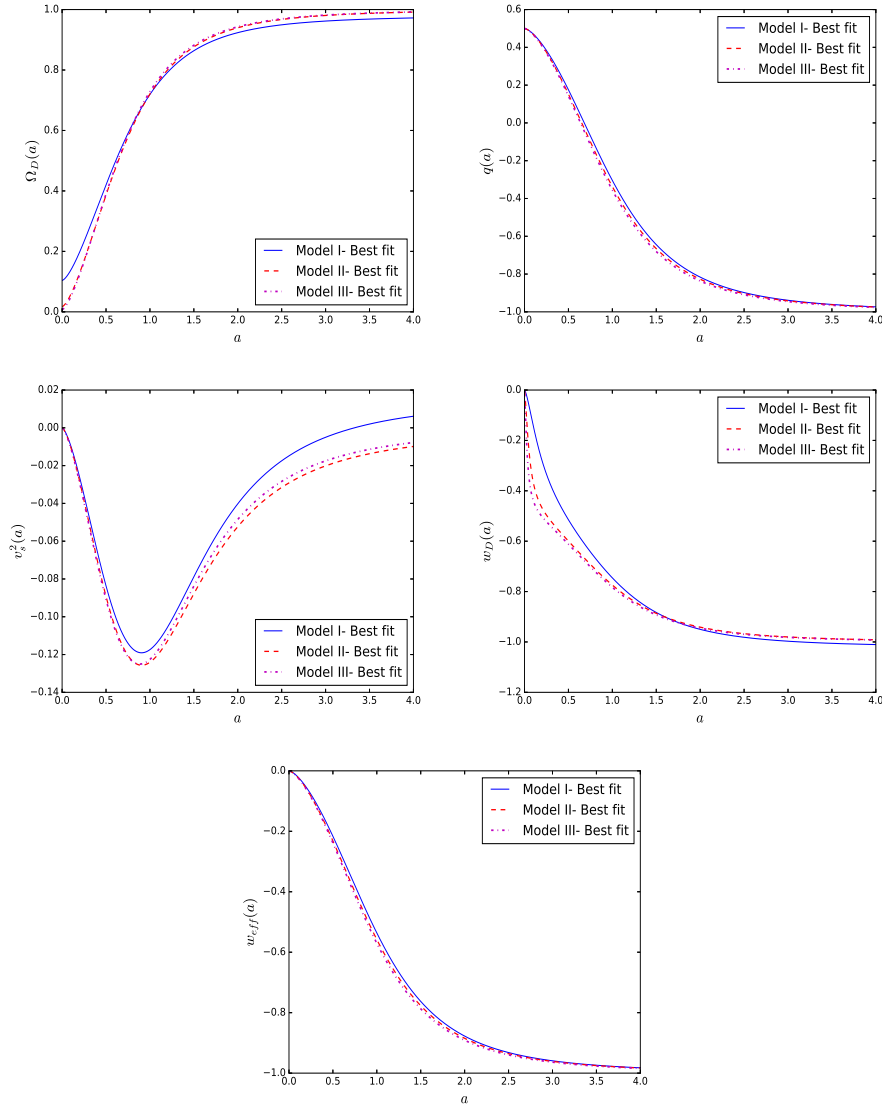


Fig. 8. The functional behavior of  $\Omega_D$ ,  $q$ ,  $v_s^2$ ,  $w_D$  and  $w_{eff}$  for model I, II and III for the best fit value of free parameters. For the first model  $\Omega_D = 0.7192^{+0.0062}_{-0.0062}$ ,  $b^2 = 0.46^{+0.030}_{-0.026}$  and  $\zeta = 0.104^{+0.047}_{-0.047}$ . For the second model  $\Omega_D = 0.7209^{+0.0065}_{-0.0065}$ ,  $b^2 = 0.0395^{+0.0080}_{-0.0080}$  and  $\zeta \leq 0.0173$  and for the third model  $\Omega_D = 0.7287^{+0.0062}_{-0.0062}$ ,  $b^2 = 0.0109^{+0.0023}_{-0.0023}$  and  $\zeta \leq 0.00764$ . Here we choose the scale factor at present time as  $a_0 = 1$ .

model goes to large negative values while for model I and II this quantity remains in interval  $w_D \in [-1, 0]$ .

## 5. Summary and Conclusion

Ghost dark energy (GDE) is one of interesting models that solves the recent acceleration problem. A great point about GDE is that this model is based on the Veneziano ghost field which has already presented in the literature and there is no need to introduce any additional degree of freedom in physics. This model also solves the coincidence problem.<sup>52</sup> However, GDE shows signs of instability (due to negativity of adiabatic squared sound speed  $v_s^2$ ) in non-interacting and linear interacting domain. It is possible to switch from GDE to the generalized ghost dark energy (GGDE) which  $\rho_D = \alpha H + \beta H^2$ . We also extended the interaction between DE and DM to non-linear regime seeking for better agreement with observations and improving the negativity of squared sound speed of the model.

To this end, we proposed three forms of non-linear interaction terms and investigated different features of these models. Generally, one can consider the functional form  $Q \equiv f(H, \rho_m, \rho_D, \rho_{tot})$  for interaction between dark sectors of the universe with a coupling coefficient denoted by  $b^2$ . We considered GGDE with non-linear interaction terms in the form  $Q = 3b^2 H \rho_D^3 / \rho^2$ ,  $Q = 3b^2 H \rho_D \rho_m / \rho$  and  $Q = 3b^2 H \rho_m^2 / \rho$  as model I, II and III, respectively. If we suppose the universe is flat, the free parameters of the models are  $\{\Omega_D, \zeta, b^2\}$ .

We evaluated the behavior of  $w_D(a)$ ,  $q(a)$ ,  $w_{eff}(a)$ ,  $\Omega_D(a)$  and  $v_s^2(a)$ . As an interesting result we found that  $v_s^2$  takes positive values at  $a > 1$  for the best fit values of parameters of the model I (Fig.8), which is a sign of stability of this model. However the squared sound speed of models II, III remains negative. Considering the variations of  $q$ ,  $w_{eff}$  (Fig.8), one can see that all models show the expected behavior of deceleration in the past and acceleration in the present time and future, in fact there is a transition from decelerating to accelerating phase at  $z = 0.69$ ,  $z = 0.67$  and  $z = 0.66$  for models I, II and III respectively. Our results also show the phantom behavior of DE in the model I at late times. In the case of third model,  $w_D$  takes large negative values at very early times but it does not affect the model due to the negligible value of  $\Omega_D$  at the early times. It is also notable that  $\Omega_D$  of the first model takes non-zero values in the early universe. This is another difference of model I and models II and III.

For observational consistency check, we used Joint Light-curve analysis (JLA) for SNIa and used Hubble parameter for different redshifts. Six observational indicators of BAO and 3 well-defined CMB parameters have been used for that purpose. For the first model, the joint analysis indicates that  $\Omega_D = 0.7192 \pm 0.0062$ ,  $b^2 = 0.146_{-0.026}^{+0.030}$  and  $\zeta = 0.104 \pm 0.047$  at 1 optimal variance error. For the second model the best fit values at  $1\sigma$  confidence are  $\Omega_D = 0.7209 \pm 0.0065$ ,  $b^2 = 0.0395 \pm 0.0080$  and  $\zeta \leq 0.0173$ . According to the combination of all observational data sets considered in this paper, the best fit values for third non-linear interacting dark energy model are  $\Omega_D = 0.7287_{-0.0062}^{+0.0062}$ ,  $b^2 = 0.0109_{-0.0023}^{+0.0023}$  and  $\zeta \leq 0.00764$  at  $1\sigma$  confidence interval. Based on  $\Delta AIC$  and  $\Delta BIC$  criteria reported in tables 6, 7 and 8 and considering  $\Lambda$ CDM model as reference cosmological model, we found that all non-linear

interacting dark energy models are compatible with current observations. Extending our approach to constraint on the models based on large scale structures and those observations beyond zero order perturbations could be interesting especially for discrimination between different models of interacting dark energy. This part of research is in progress and we will be addressing them later.

### Acknowledgment

The work of E. Ebrahimi has been supported financially by Research Institute for Astronomy and Astrophysics of Maragha (RIAAM) under project No. 1/4165-55.

### References

1. A. G. Riess *et al.* [Supernova Search Team Collaboration], *Astron. J.* **116**, 1009 (1998) doi:10.1086/300499 [astro-ph/9805201].
2. S. Perlmutter *et al.* [Supernova Cosmology Project Collaboration], *Astrophys. J.* **517**, 565 (1999) doi:10.1086/307221 [astro-ph/9812133].
3. P. de Bernardis, *et al.*, *Nature* **404** (2000) 955.
4. S. Perlmutter, *et al.*, *Astrophys. J.* **598** (2003) 102;
5. S. Hanany *et al.*, *Astrophys. J. Lett.* **545**, L5 (2000);
6. C. B. Netterfield *et al.*, *Astrophys. J.* **571**, 604 (2002);
7. D.N. Spergel *et al.*, *Astrophys. J. Suppl.* **148**, 175 (2003).
8. P. A. R. Ade *et al.* [Planck Collaboration], arXiv:1502.01590 [astro-ph.CO].
9. M. Colless *et al.*, *Mon. Not. R. Astron. Soc.* **328**, 1039 (2001);
10. M. Tegmark *et al.*, *Phys. Rev. D* **69**, 103501 (2004);
11. S. Cole *et al.*, *Mon. Not. R. Astron. Soc.* **362**, 505 (2005);
12. V. Springel, C.S. Frenk, and S.M.D. White, *Nature (London)* **440**, 1137 (2006).
13. W. J. Percival *et al.* [SDSS Collaboration], *Mon. Not. Roy. Astron. Soc.* **401**, 2148 (2010) doi:10.1111/j.1365-2966.2009.15812.x [arXiv:0907.1660 [astro-ph.CO]].
14. C. Blake *et al.*, *Mon. Not. Roy. Astron. Soc.* **415**, 2876 (2011) doi:10.1111/j.1365-2966.2011.18903.x [arXiv:1104.2948 [astro-ph.CO]].
15. B. A. Reid *et al.*, *Mon. Not. Roy. Astron. Soc.* **426**, 2719 (2012) doi:10.1111/j.1365-2966.2012.21779.x [arXiv:1203.6641 [astro-ph.CO]].
16. V. Sahni and A. A. Starobinsky, *Int. J. Mod. Phys. D* **9**, 373 (2000) doi:10.1142/S0218271800000542 [astro-ph/9904398].
17. S. M. Carroll, *Living Rev. Rel.* **4**, 1 (2001) doi:10.12942/lrr-2001-1 [astro-ph/0004075].
18. E. J. Copeland, M. Sami and S. Tsujikawa, *Int. J. Mod. Phys. D* **15**, 1753 (2006) doi:10.1142/S021827180600942X [hep-th/0603057].
19. O. Luongo, H. Quevedo, *Int. J. Mod. Phys. D*, **23**, 1450012, pp. 8, (2014).
20. A. De Felice and S. Tsujikawa, *Living Rev. Rel.* **13**, 3 (2010) doi:10.12942/lrr-2010-3 [arXiv:1002.4928 [gr-qc]].
21. S. Tsujikawa, *Lect. Notes Phys.* **800**, 99 (2010) doi:10.1007/978-3-642-10598-2-3 [arXiv:1101.0191 [gr-qc]].
22. T. Clifton, P. G. Ferreira, A. Padilla and C. Skordis, *Phys. Rept.* **513**, 1 (2012) doi:10.1016/j.physrep.2012.01.001 [arXiv:1106.2476 [astro-ph.CO]].
23. Amendola, L., Appleby, S., Bacon, D., *et al.*, *Cosmology and fundamental physics with the Euclid satellite*. 2012a, ArXiv e-prints, arXiv:1206.1225
24. J. Sola and H. Stefancic, *Phys. Lett. B* **624**, 147 (2005).
25. C. Wetterich, *Nucl. Phys. B* **302** (1988) 668;

26. B. Ratra, J. Peebles, Phys. Rev. D 37 (1988) 321.
27. S. Dutta, E. N. Saridakis and R. J. Scherrer, Phys. Rev. D 79, 103005 (2009).
28. E. N. Saridakis and S. V. Sushkov, Phys. Rev. D 81, 083510 (2010).
29. S. Rahvar and M. S. Movahed, Phys. Rev. D **75**, 023512 (2007)  
doi:10.1103/PhysRevD.75.023512 [astro-ph/0604206].
30. R. R. Caldwell, Phys. Lett. B 545, 23 (2002).
31. S. Nojiri and S. D. Odintsov, Phys. Lett. B 562, 147 (2003)
32. P. Singh, M. Sami and N. Dadhich, Phys. Rev. D 68, 023522 (2003).
33. W. Hu, Phys. Rev. D 71, 047301 (2005).
34. M. R. Setare and E. N. Saridakis, JCAP 0903, 002 (2009).
35. E. N. Saridakis, Nucl. Phys. B 819, 116 (2009).
36. S. D. H. Hsu, Phys. Lett. B 594, 13 (2004).
37. M. Li, Phys. Lett. B 603, 1 (2004).
38. Q. G. Huang and M. Li, JCAP 0408, 013 (2004).
39. E. Elizalde, S. Nojiri, S. D. Odintsov and P. Wang, Phys. Rev. D 71, 103504 (2005)
40. E. N. Saridakis, Phys. Lett. B 660, 138 (2008)
41. E. N. Saridakis, JCAP 0804, 020 (2008).
42. R.G. Cai, Phys. Lett. B 657, 228 (2007).
43. H. Wei and R.G. Cai, Phys. Lett. B 660, 113 (2008).
44. H. Wei and R.G. Cai, Eur. Phys. J. C 59, 99 (2009)
45. F. R. Urban and A. R. Zhitnitsky, Phys. Lett. B 688 (2010) 9 ;Phys. Rev. D 80 (2009)  
063001; JCAP 0909 (2009) 018; Nucl. Phys. B 835 (2010) 135.
46. N. Ohta, Phys. Lett. B 695 (2011) 41, arXiv:1010.1339.
47. K. Kawarabayashi and N. Ohta, Nucl. Phys. B 175, 477 (1980).
48. E. Witten, Nucl. Phys. B 156 (1979) 269;
49. G. Veneziano, Nucl. Phys. B 159 (1979) 213.
50. C. Rosenzweig, J. Schechter and C. G. Trahern, Phys. Rev. D 21 (1980) 3388.
51. P. Nath and R. L. Arnowitt, Phys. Rev. D 23 (1981) 473.
52. R.G. Cai, Z.L. Tuo, H.B. Zhang, arXiv:1011.3212.
53. A. Sheykhi, A. Bagheri, Europhys. Lett. 95, 39001 (2011).
54. E. Ebrahimi, A. Sheykhi, Phys. Lett. B 705, 19 (2011).
55. E. Ebrahimi, A. Sheykhi, Int. J. Mod. Phys. D 20, 2369 (2011)
56. A. Sheykhi, M. Sadegh Movahed, Gen. Relativ. Gravit. [DOI:10.1007/s10714-011-1286-3].
57. Chao-Jun Feng, Xin-Zhou Li, Ping Xi, JHEP 1205(2012) 046.
58. Chao-Jun Feng, Xin-Zhou Li, Xian-Yong Shen, Phys.Rev. D87 (2013) 023006.
59. Chao-Jun Feng, Xin-Zhou Li, Xian-Yong Shen, Mod. Phys. Lett. A27 (2012) 1250182.
60. R. G. Cai, Z. L. Tuo, Y. B. Wu, Y. Y. Zhao, Phys. Rev. D 86 (2012) 023511.
61. E. Ebrahimi, A. Sheykhi and H. Alavirad, Central Eur. J. Phys. **11**, no. 7, 949 (2013).
62. Bertolami O, Gil Pedro F and Le Delliou M 2007 Phys. Lett. B 654 165.
63. G. Olivares, F. Atrio, D. Pavon, Phys. Rev. D 71 (2005) 063523.
64. G. Mangano, G. Miele, and V. Pettorino, Mod.Phys.Lett. A 18, 831 (2003),  
arXiv:astro-ph/ 0212518.
65. M. Baldi, Mon.Not.Roy.Astron.Soc. 411,1077 (2011), arXiv:1005.2188
66. Jian-Hua He and Bin Wang, JCAP 0806, 010 (2008).
67. F. Arevalo, A. P. R. Bacalhau and W. Zimdahl, Class. Quant. Grav. **29**, 235001 (2012)
68. N. Afshordi, C. Coriano, L. Delle Rose, E. Gould, K. Skenderis, Phys. Rev. Lett. 118,  
041301 (2017)
69. C.-Qiang Geng, C.-Chi Lee, K. Zhang, Phys. Lett. B 757 (2016) 422-427
70. R. R. Cuzinatto, L. G. Medeiros, E. M. de Moraes, Astroparticle Physics 73 (2016) 52

30 *E. Ebrahimi, H. Golchin, A. Mehrabi, S. M. S. Movahed*

71. A. Aviles, C. Gruber, O. Luongo, H. Quevedo, Phys.Rev.D86, 123516 (2012)
72. S. Rani, A. Altaibayeva, M. Shahalam, J. K. Singh, R. Myrzakulov, JCAP 03 (2015) 031
73. M. Moresco, L. Verde, L. Pozzetti, R. Jimenez, A. Cimatti, JCAP, 07, 053, (2012)
74. A. de la Cruz-Dombriz, P. K. S. Dunsby, O. Luongo, L. Reverberi, Jour. Cosmo. Astrp. Phys., 12, 042, pp. 32, (2016).
75. Y. Chen, S. Kumar, B. Ratra, Astrophys.J. 835 (2017) 86
76. I. Semiz, A. Kazim Camlibel, JCAP 1512 (2015) no.12, 038
77. M. B. Gavela, D. Hernandez, L. L. Honorez, O. Mena, and S. Rigolin, JCAP 0907 (2009) 034, [0901.1611].
78. E. Majerotto, J. Valiviita, and R. Maartens, 0907.4981.
79. E. Ebrahimi, A. Sheykhi, Int J Theor Phys (2013) 52:29661776.
80. H. Golchin, S. Jamali and E. Ebrahimi, arXiv:1605.05068 [gr-qc].
81. G. Hinshaw *et al.* [WMAP Collaboration], Astrophys. J. Suppl. **208**, 19 (2013)
82. P. A. R. Ade *et al.* [Planck Collaboration], arXiv:1502.01589 [astro-ph.CO].
83. A. G. Riess *et al.*, ApJ. 607 (2004) 665.
84. A. G. Riess *et al.*, ApJ. 659 (2007) 98.
85. P. Astier *et al.*, Astron. Astrophys. 447 (2006) 31;
86. S. Baumont *et al.*, Astron. Astrophys. 491 (2008) 567.
87. N. Regnault *et al.*, arXiv:0908.3808
88. J. Guy *et al.*, arXiv:1010.4743.
89. G. Miknaitis *et al.*, ApJ. 666 (2007) 674
90. W. M. Wood-Vasey *et al.*, ApJ. 666 (2007) 694.
91. Y. Copin *et al.*, New Astronomy Rev. 50 (2006) 436
92. R. A. Scalzo *et al.*, ApJ. 713 (2009) 1073
93. G. Folatelli *et al.*, AJ. 139 (2010) 120
94. G. Folatelli *et al.*, AJ. 139 (2010) 519.
95. J. Leaman *et al.*, arXiv:1006.4611
96. W. D. Li *et al.*, arXiv:1006.4612; W. D. Li *et al.*, arXiv:1006.4613.
97. J. A. Holtzman *et al.*, AJ. 136 (2008) 2306
98. R. Kessler *et al.*, ApJS. 185 (2009) 32.
99. Suzuki, N., *et al.* 2012, ApJ, 746, 85
100. S. Cao and Z. H. Zhu, Phys. Rev. D **90**, no. 8, 083006 (2014)
101. M. Betoule *et al.* [SDSS Collaboration], Astron. Astrophys. 568 (2014) A22 [arXiv:1401.4064 [astro-ph.CO]].
102. <http://supernova.lbl.gov/Union/>
103. [http://supernovae.in2p3.fr/sdss\\_snls\\_jla/ReadMe.html](http://supernovae.in2p3.fr/sdss_snls_jla/ReadMe.html)
104. Li, Z. X., Wu, P. X., & Yu, H. W. 2011, PLB, 695, 1
105. O. Farooq and B. Ratra, Astrophys. J. 766, L7 (2013)
106. Padmanabhan, N., *et al.*, Mon. Not. Roy. Astron. Soc. **427**, 2132 (2012)[arXiv:1202.0090].
107. Anderson, L., *et al.*, Mon. Not. Roy. Astron. Soc. **427**, 3435 (2013)[arXiv:1203.6594].
108. Blake, C., *et al.* 2012, MNRAS, 425, 405
109. Beutler, F., *et al.* 2011, MNRAS, 416, 3017
110. C. Blake *et al.*, Mon. Not. Roy. Astron. Soc. **418**, 1707 (2011)
111. Hu, W., & Sugiyama, N. 1996, ApJ, 471, 542
112. H. Akaike, A new look at the statistical model identification, IEEE Trans. Automatic Control 19, 716 (1974).
113. G. Schwarz, Estimating the dimension of a model. Ann. Stat. 6, 461 (1978)
114. Y. Y. Xu and X. Zhang, arXiv:1607.06262 [astro-ph.CO].